Key Role of a Threefold State Crossing in the Ultrafast Decay of Electronically Excited Cytosine

Lluís Blancafort*,[†] and Michael A. Robb[‡]

Institut de Química Computacional and Departament de Química, Universitat de Girona, E-17071 Girona, Spain, and Department of Chemistry, Imperial College London, South Kensington Campus, London SW7 2AZ, United Kingdom

Received: September 6, 2004

A three-state conical intersection between the ground state and the (π,π^*) and (n_O,π^*) singlet excited states of cytosine is the topological feature that dominates the ultrafast decay of singlet excited cytosine. The three-state intersection is associated with seams of intersection between pairs of states (S_1/S_0 and S_2/S_1, respectively), and the resulting topology has been mapped out with CASSCF and CAS-PT2 calculations. The minimum-energy path for the optically active (π,π^*) state lies on the S_1 surface, and decay to the ground state takes place at the S_1/S_0 seam. On the other hand, the region of the S_2/S_1 seam must be traversed before accessing the conical intersection with the ground state and recrossing to S_2 becomes possible. Another feature associated with the three-state degeneracy is vibronic coupling between the (π,π^*) and (n_O,π^*) excited states (proximity effect), which lowers the barrier to the S_1/S_0 seam. From a mechanistic point of view, then, the decay is the outcome of the interaction between the three states. The results also suggest that the experimental excited-state lifetime is the effect of two factors, an energetically accessible region of S_1/S_0 degeneracy and a region where the decay can be slowed because of recrossing to S_2.

Introduction

The photophysics of cytosine and the remaining DNA and RNA bases and nucleosides in the gas phase and in solution is characterized by ultrashort excited-state lifetimes in the femtosecond and low picosecond range.[1−10] A recent CASSCF theoretical investigation of the photophysics of the singlet-excited cytosine base has shown that the decay involves the passage through a surface crossing (conical intersection) between the excited and the ground states of the molecule, $(S_1/S_0)_X$.[11,12] One factor responsible for the ultrafast lifetimes is the fact that the minimum-energy path (MEP) to the surface crossing is associated with a low energy barrier. In the present study, we introduce a second feature of the PES that is essential for the ultrafast decay, namely, the presence of an extensive region of S_1/S_0 intersection. More importantly, the PES contains a three-state degeneracy, $(S_2/S_1/S_0)_X$, between the three relevant states: the ground state and the (π,π^*) and (n_O,π^*) (excitation coming from the oxygen lone pair) excited states (Figure 1), found at the CASSCF level of theory and confirmed at the CAS-PT2 level.

Three-state degeneracies of the same multiplicity are known for cases imposed by symmetry,[13,14] such as the radical cation of methane[15,16] and transition-metal complexes.[17,18] Ultrafast relaxation through a symmetry-imposed 3-fold degeneracy has been observed for $Fe(CO)_4$.[19] Examples not imposed by symmetry have been recently identified by the group of Yarkony for the excited states of several organic molecules.[20−23] Three-state conical intersections have a five-dimensional branching space (i.e., they form an (N-5)-dimensional subspace, where N is the number of vibrational degrees of freedom of the molecule), in contrast to two-state intersections, which belong to an (N-2)-dimensional subspace. In this paper, we focus on the potential-energy surface that is generated around a three-state conical intersection found in cytosine. The relevant point is that the triple crossing is associated with an intersection space composed of several linked seams between pairs of states.[21,24,25] In cytosine, this implies that the triple crossing is associated with S_1/S_0 and S_2/S_1 seams of degeneracy, which we have characterized. As a consequence, decay to the ground state is not limited to the calculated MEP through the $(S_1/S_0)_X$ minimum-energy structure of the doubly degenerate space (see Figure 2, where the S_1/S_0 seam is the full curve on the S_1 surface). Depending on the relative energetics and the dynamics, it can take place along a segment of that intersection space, as it is known from previous dynamics calculations on other systems.[26−28] This explains the ultrafast excited-state lifetimes measured experimentally. On the other hand, the decay path goes near a region of S_2/S_1 degeneracy before reaching the region of decay to the ground state (dashed line in Figure 2). Nonadiabatic recrossing from the spectroscopically active S_1 state to S_2 is possible and can eventually slow the decay rate. In this context, the decay of cytosine takes place on the ultrafast time scale (approximately 3.2 ps for the monoexponential decay of the

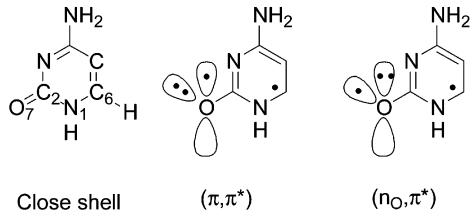

Figure 1. Resonance structures for the three relevant singlet excited states in cytosine ultrafast decay.

* Corresponding author. E-mail: lluisb@stark.udg.es.
[†] Universitat de Girona.
[‡] Imperial College London.

10.1021/jp045985b CCC: $27.50
Published on Web 10/30/2004

TABLE 1: Energetics and Structures of Critical Points at CASSCF/6-31G* and CAS-PT2/6-31G* Levels

	CASSCF					CAS-PT2				
structure	energy[a] [kcal mol^{-1}]	energy[a] [eV]	r_{C2-O7}[b] [Å]	pyr_{C6}[c] [deg]	pyr_{N1}[d] [deg]	energy[a] [kcal mol^{-1}]	energy[a] [eV]	r_{C2-O7}[b] [Å]	pyr_{C6}[c] [deg]	pyr_{N1}[d] [deg]
FC	38.4 (π,π^*)	1.67	1.201	0	0	18.2 (π,π^*)	0.79	1.201	0	0
	38.7 (n_O,π^*)	1.68				27.0 (n_O,π^*)	1.17			
$(S_1)_{Min}$	0.0 (n_O,π^*)	0.00	1.340	20	12	0.0 (π,π^*)	0.00	1.331	21	5
$(S_1/S_0)_X$	3.6	0.16	1.408	37	18	−0.6	−0.03	1.418	37	18
$(S_2/S_1)_X$	3.3	0.14	1.331	21	5	6.6[e]	0.29	1.385	33	14
$(S_2/S_1/S_0)_X$	13.8[f]	0.60	1.423	19	0	55.7[g]	2.42	1.513	20	0

[a] Relative to $(S_1)_{Min}$, see Computational Details for active spaces. [b] C_2-O_7 bond length. [c] Pyramidalization of C_6 atom (see Computational Details). [d] Pyramidalization of N_1 atom (see Computational Details). [e] Corresponds to the barrier along the MEP (Figure 4). [f] Relative energies of the three states: 11.7, 14.0, and 15.8 kcal mol^{-1}. [g] Relative energies of the three states: 55.5, 55.7, and 55.8 kcal mol^{-1}.

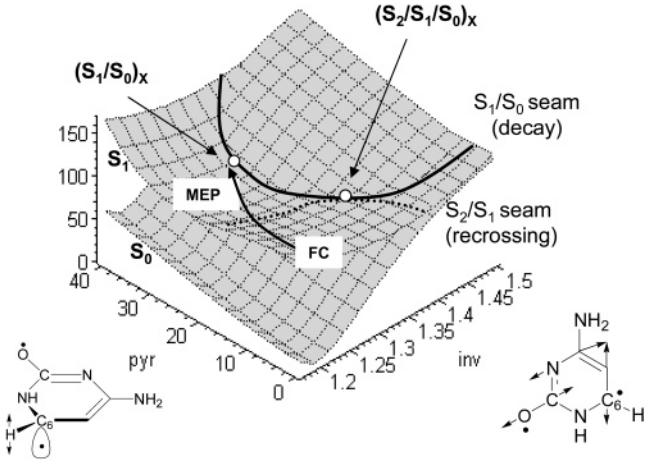

Figure 2. Two-coordinate sketch of the potential energy surface for the ground and the excited state (S_1) of cytosine along the bond inversion (inv) and pyramidalization (pyr) coordinates, showing the S_1/S_0 and S_2/S_1 seams of intersection and the minimum-energy path (MEP).

base in the gas phase), but the decay of the purine bases is several times faster (approximately 1.0 and 0.8 ps for adenine and guanine in the gas phase, respectively).[3] Recrossing to S_2 might explain the comparably slower decay of cytosine.

The present results shed additional light on the role of the (n_O,π^*) and (π,π^*) states in the radiationless decay. Reconsideration of the wave function for the three relevant states (ground state and both excited ones) shows that the distinction between the two excited states is blurred in the region of decay to the ground state. The states have a mixed character there due to vibronic interaction along the pyramidalization coordinate, which breaks the plane of symmetry of the molecule. This manifestation of the proximity effect between the (π,π^*) and (n_O,π^*) states induces a lowering of the energy of S_1 reflected in the energy lowering for the S_1/S_0 seam along the pyramidalization mode. The role of the proximity effect in lowering the barrier for ultrafast decay in the photophysics of the DNA nucleosides (mainly adenine) has been proposed previously on the base of experimental[3,5,29] and theoretical[30] studies. Our results show the importance of this effect in the photophysics of cytosine and prove that the topology of the PES is generated by the interplay between ground state and both excited states.

Computational Details

The CASSCF calculations were carried out with the Gaussian98 package of programs,[31] while the CAS-PT2 energetics were recalculated with MOLCAS.[32] All calculations use the 6-31G* basis set, with the exception of the calculation to determine the pseudo-Jahn−Teller effect (see Supporting Information). The CASSCF wave function used for the CAS-PT2 calculations was a three-state calculation, state-averaging over the three states (factors 3 × 0.33), with a (12, 9) active space (all π-type orbitals and the oxygen nonbonding n_O orbital).

The optimization of the critical points at the CASSCF level is described in our previous theoretical study of cytosine photophysics.[11] $(S_1)_{Min,CAS}$ (at the CASSCF level) is structure $(n_O,\pi^*)_{Min}$ from our previous study, whereas $(S_1)_{Min,PT2}$ (at the CAS-PT2 level)[12] is structure $(\pi,\pi^*)_{Min}$ (obtained at the CASSCF level). The structures $(S_1/S_0)_{X,CAS}$ and $(S_2/S_1)_{X,CAS}$, optimized at the CASSCF level, are the structures $(GS/n_O,\pi^*)_{CI}$ and $(n_O,\pi^*/\pi,\pi^*)_{CI}$ from our previous study, respectively.

The relevant energetics and geometric parameters of the structures (C_2-O_7 bond length and pyramidalization at C_6 and N_1) are collected in Table 1. The pyramidalization angle of C_6 is defined as the difference between the $H-C_6-C_5-N_1$ dihedral angle and 180° (reference angle at planar geometries). For the pyramidalization at N_1, the $H-N_1-C_2-C_6$ dihedral is used analogously. The energetics are given relative to the energy of $(S_1)_{Min}$.

The surface topologies presented in Figures 2 and 3 are based on CASSCF and CAS-PT2 results obtained in part with nonstandard procedures (linear interpolations and linear displacements along calculated CASSCF gradients). These procedures are described succinctly here, and the details are given in the Supporting Information. To map out the decay coordinate at the CAS-PT2 level, the crossing between the ground and the first excited state, $(S_1/S_0)_{X,PT2}$, was located starting from the CASSCF-optimized intersection $(S_1/S_0)_{X,CAS}$, following the gradient-difference coordinate (difference between gradients of S_1 and S_0, at the CASSCF level) at that point (see Figure S1, Supporting Information). This procedure is similar to the one followed in the previous CAS-PT2 study,[12] and the CAS-PT2 crossing occurs between S_0 and S_2 CASSCF states. The approach used here is possible because the wave functions of the states at $(S_1/S_0)_{X,CAS}$ correspond, approximately, to the ground state and the excited state. At $(S_1/S_0)_{X,CAS}$, the gradient of S_1 is approximately zero, and the gradient difference is essentially equal to the ground-state gradient (the gradient of S_2, which is the state degenerate with S_0 at the CAS-PT2 level, is also approximately zero). The gradient difference corresponds to bond inversion (see the inset of Figure S1).

To obtain the MEP at the CAS-PT2 level (see Figure 4), the decay coordinate between the two relevant points, $(S_1/S_0)_{X,PT2}$ and $(S_1)_{Min,PT2}$, is determined at the CASSCF level by running an intrinsic reaction coordinate (IRC)[33] in the full space of nuclear coordinates (see Supporting Information for details). The CAS-PT2 energetics are recalculated along the CASSCF coordinate, which corresponds approximately to concerted bond inversion and C_6 pyramidalization. The barrier along the IRC profile is 6.6 kcal mol^{-1} (0.29 eV) and the fact that the CAS-

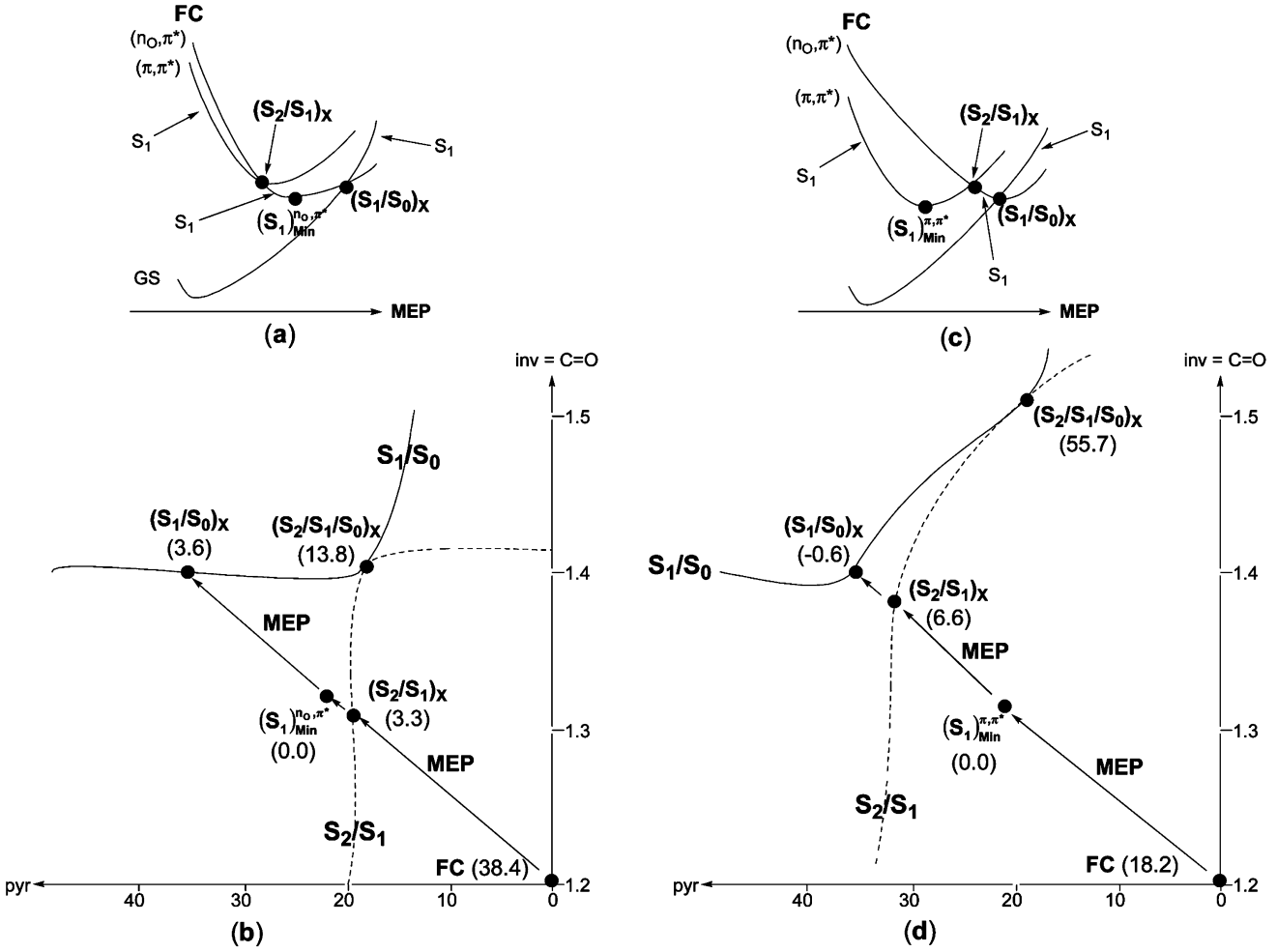

Figure 3. Projections of the cytosine potential energy surface (CASSCF and CAS-PT2 energetics in kcal mol^{-1}). (a and c) One-dimensional profiles along MEP, CASSCF, and CAS-PT2 energetics, respectively. (b and d) Two-coordinate projections of S_1 states along the bond inversion (inv, represented by the C_2-O_7 bond length) and C_6 pyramidalization (pyr) coordinates, CASSCF, and CAS-PT2 energetics, respectively.

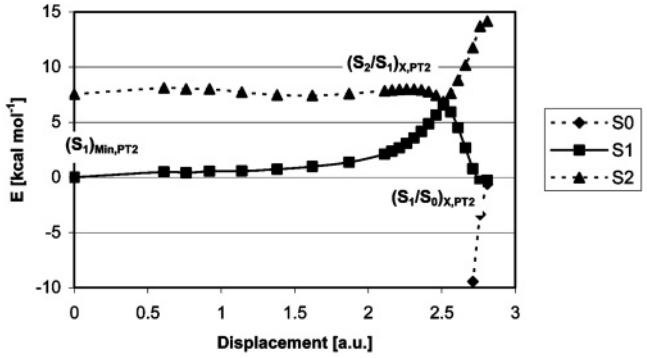

Figure 4. CAS-PT2 energy profile (energies relative to $(S_1)_{Min,PT2}$) along the MEP from $(S_1/S_0)_{X,PT2}$ to $(S_1)_{Min,PT2}$.

PT2 profile goes through a point of S_1/S_2 degeneracy, named $(S_2/S_1)_{X,PT2}$ here (Figure 4), shows the similarity with the CASSCF results. The methodology followed here is more rigorous than the one used previously in the determination of the decay barrier at the CAS-PT2 level, based on constrained CASSCF optimizations at fixed C_2-O_7 distances (relaxed scan).[12] Following this procedure, the first structure along the coordinate, starting from $(S_1/S_0)_{X,PT2}$, is obtained from a constrained optimization at fixed C_2-O_7 distance of 1.41 Å (the C_2-O_7 distance at $(S_1/S_0)_{X,PT2}$ is 1.418 Å). The optimized structure, $(S_1)_{1.41}$, is approximately 1.7 atomic units away from $(S_1/S_0)_{X,PT2}$. This step is too large, and to complete the path it is necessary to carry out an interpolation between $(S_1)_{1.41}$ and $(S_1/S_0)_{X,PT2}$, which differ in the bond distances in the ring and the pyramidalization angles at C_6 (approximately 14° at $(S_1)_{1.41}$ against 35° at $(S_1/S_0)_{X,PT2}$). This interpolation (Figure S2, Supporting Information) shows the presence of a barrier of approximately 7 kcal mol^{-1} (0.30 eV) associated with an S_2/S_1 crossing, along the previously unexplored part of the path. Without this interpolation, the path obtained by a relaxed scan[12] is incomplete, and the previously reported barrier (2.5 kcal mol^{-1}) is incorrect. However, a linear interpolation between $(S_1/S_0)_{X,PT2}$ and $(S_1)_{Min,PT2}$ gives the same qualitative CAS-PT2 profile[12] than the IRC-based one shown in Figure 4.

A point in the subspace of triple degeneracy, $(S_2/S_1/S_0)_{X,CAS}$, is found by displacing structure $(S_2/S_1)_{X,CAS}$ (labeled $(n_O,\pi^*/\pi,\pi)_{CI}$ in our previous communication)[11] along a coordinate GD′ obtained by subtracting the ground-state gradient from the average of the two excited-state gradients at $(S_2/S_1)_X$, that is,

$$GD' = \frac{1}{2}(g_{S1} + g_{S2}) - g_{S0}$$

where g_i are the gradients of the states (see Figure 5). The coordinate corresponds mainly to bond inversion at constant C_6 pyramidalization angle (see the inset of Figure 5). The method used here to locate the triple crossing takes advantage of the fact that the S_2 and S_1 states have similar gradients. Thus, displacement along the GD′ coordinate will approximately retain

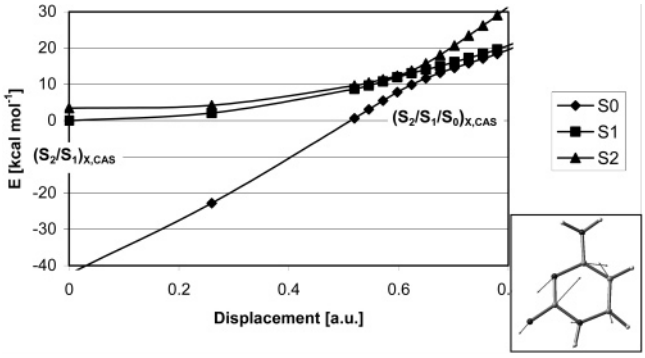

Figure 5. CASSCF energy profile (energies relative to $(S_1)_{Min,CAS}$) along the GD′ coordinate (see Computational Details), starting at $(S_2/S_1)_{X,CAS}$.

TABLE 2: Configurations of the S_0-S_2 States at the $(S_1/S_0)_{X,PT2}$ Decay Point (Squares of CASSCF Eigenvectors)

state	CS[a]	(π,π^*)	(n_O,π^*)
S_0 [b]	0.23	0.32	0.25
S_1	0.02	0.45	0.40
S_2 [b]	0.42	0.09	0.21

[a] Closed-shell wave function (approximately correlated with ground state at Franck−Condon geometry). [b] S_2 and S_0 states degenerate at CAS-PT2 level.

the S_2/S_1 degeneracy, whereas the gap between the two states and S_0 will be reduced. This procedure does not guarantee that the triple crossing space is located, but a point of near-degeneracy between the three states is found, with energy gaps of 2.3 kcal mol^{-1} between S_0 and S_1, and 1.8 kcal mol^{-1} between S_1 and S_2, at the CASSCF level. The energy of this structure, $(S_2/S_1/S_0)_{X,CAS}$, is approximately 14 kcal mol^{-1} (0.6 eV) higher than $(S_1)_{Min}$ and well below the vertical excitation (by approximately 24 kcal mol^{-1} or 1.0 eV, see Table 1). This structure is not the optimized triple degeneracy at the CASSCF level, but a lower bound to its energy is given by the energy of the optimized $(S_1/S_0)_{X,CAS}$ structure. An algorithm for the optimization of 3-fold degenerate points was recently presented by Yarkony,[23,34] and we are currently developing a similar algorithm on the basis of the conical−intersection optimization algorithm implemented in Gaussian.[35] At the CAS-PT2 level (see Figure S3, Supporting Information), $(S_2/S_1/S_0)_{X,PT2}$ is found further along the GD′ coordinate (for example, the C−O bond is stretched to approximately 1.51 Å against 1.41 Å at $(S_2/S_1/S_0)_{X,CAS}$), and the three states lie within a range of 0.3 kcal mol^{-1}. The energy of $(S_2/S_1/S_0)_{X,PT2}$ relative to $(S_1)_{Min,PT2}$ is remarkably higher than the corresponding value at the CASSCF level (approximately 56 kcal mol^{-1} or 2.4 eV, see Table 2), presumably because it was located using the GD′ coordinate based on the CASSCF gradients.

The S_2/S_1 and S_1/S_0 seams of intersection shown in Figures 2 and 3 were characterized by linear interpolation between the $(S_2/S_1/S_0)_X$ structure and the $(S_2/S_1)_X$ and $(S_1/S_0)_X$ ones, respectively, both at the CASSCF and CAS-PT2 levels of theory (see Supporting Information for details, Figures S4−S6). These linear interpolations give approximate cuts of the 2-fold degenerate space along one coordinate.

For the interpretation of the states involved in the decay (assignment of (π,π^*) and (n_O,π^*) character), we have reanalyzed the configurations for the wave functions of the three relevant states along the MEP from $(S_1)_{Min,PT2}$ to $(S_1/S_0)_{X,PT2}$. The states are characterized in terms of the three dominant configurations: a closed-shell one that corresponds approximately to the ground state, a (n_O,π^*) excited one, and a (π,π^*) excited one (see the squares of the CASSCF eigenvector coefficients in Table 2). As the path approaches the decay point $(S_1/S_0)_{X,PT2}$, the states mix and the wave functions become multireferential (see Figures S7−S9, Supporting Information). At $(S_1/S_0)_{X,PT2}$, the three configurations have approximately the same weights (0.25−0.3) for S_0, although the (π,π^*) configuration dominates slightly. In turn, S_2 (degenerate with S_0 at the CAS-PT2 level) is dominated by the ground-state configuration (approximately 0.4), with an (n_O,π^*) contribution of approximately 0.2.

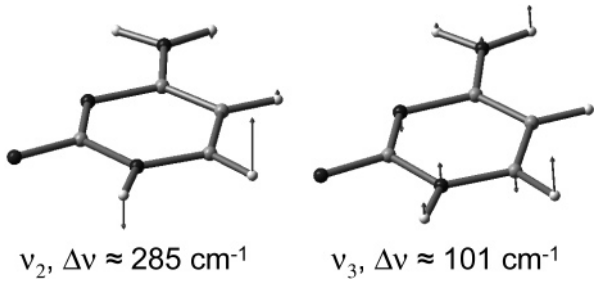

Figure 6. Lowest frequencies of (π,π^*) state minimum (constrained to C_s symmetry) and estimated contribution of vibronic coupling $(\Delta\nu)$ with the (n_O,π^*) state.

For the determination of the PJT effect, a symmetry-constrained optimization of the (π,π^*) state was carried out (C_s symmetry), and the frequency was calculated analytically. The frequency calculation was carried out using the default wave function, which includes all spin-adapted configurations, and was repeated with a symmetry-restricted wave function. The latter calculation gives the frequencies without the PJT contribution, ant the PJT effect is obtained by comparing the frequencies obtained in the two cases.[36] In the default calculation, the C_s-minimum has two imaginary frequencies of −551 and −99.4 cm^{-1} and a lowest real frequency of 128.0 cm^{-1}. The first mode corresponds to pyramidalization of the amino group, while the other two modes are linear combinations of the C_6 and N_1 ring pyramidalizations (see Figure 6). When the PJT coupling to the (n_O,π^*) state is switched off, the frequency for the amine pyramidalization remains unaltered, but the ones for the C_6 and N_1 pyramidalization modes increase to 182.1 and 229.2 cm^{-1}. This proves that pyramidalization in the (π,π^*) state is partly caused by PJT coupling. There is a further vibration that shows a substantial increase when the PJT effect is excluded from the frequency calculation, namely, a mode composed of puckering of C_2 and N_3 whose frequency changes from 745.3 to 921.8 cm^{-1}. However, the largest effect on the surface of S_1 will come from the two low-frequency modes.

Results and Discussion

Description of the Topology. In Figures 2 and 3 we present sketches of the topography for the radiationless decay of singlet excited cytosine centered on the three-state intersection. The two relevant coordinates are bond inversion and pyramidalization of the C_6 ring carbon (see Figure 1). Figure 2 gives a three-dimensional view of the S_0 and S_1 states, and projections on one and two coordinates are shown in Figure 3. The 2-fold degenerate seams (lines) and the triple crossing points of Figures 2 and 3 are projections of $(N-2)$- and $(N-5)$-dimensional subspaces on the two coordinates. This implies that the branching spaces of the crossings are not fully represented. Therefore, in our presentation, we are neglecting additional seams of 2-fold degeneracy that come out of the 3-fold degeneracy point, along some of the remaining branching-space coordinates. However, from our calculations, we find that the

coordinates of choice are the best option to give an overall view of the topography of the critical points.

Figure 3a,b is based on results obtained at the CASSCF level. However, recent computations have shown the importance of the CAS-PT2 correction (dynamic correlation) for the relative energies of the excited states of cytosine.[12] The main effect is to lower the energy of the (π,π^*) state with respect to the (n_O,π^*) state (compare Figure 3a,c). This changes the topography of the seams of double degeneracy and the relative energetics, but it does not affect the main characteristic of radiationless decay induced by interaction between three states. We now describe the surfaces in some detail.

Figure 3a shows the one-dimensional energy profile along the MEP at the CASSCF level (see our previous communication[11]). The MEP lies on the first-excited-state surface (S_1) and is characterized by a change from the spectroscopically active (π,π^*) state to the (n_O,π^*) state before the decay point to the ground state, $(S_1/S_0)_X$. The change of state is associated with a crossing between the two excited states, $(S_2/S_1)_X$. The minimum for S_1, $(S_1)_{Min}$, has (n_O,π^*) character. The reaction coordinate is a combination of bond inversion and pyramidalization of the C_6 ring carbon, and the structures $(S_1)_{Min}$ and $(S_2/S_1)_X$ lie approximately halfway between the Franck−Condon geometry and the decay point $(S_1/S_0)_X$. The main conceptual point of interest is that the two state crossings $(S_2/S_1)_X$ and $(S_1/S_0)_X$ belong to (N-2)-dimensional seams of degeneracy that cross at the triple degeneracy point $(S_2/S_1/S_0)_X$. The linkage at $(S_2/S_1/S_0)_X$ is shown in Figure 3b, which is a projection of the S_1 surface on the plane of the two relevant coordinates (the C_2-O_7 bond length is used as representative of bond inversion). The projection shows the position of the 3-fold crossing and the associated seams with respect to the MEP in that space. The S_1/S_0 seam (continuous lines in Figure 2 and Figure 3b) lies essentially along the pyramidalization coordinate, whereas the S_2/S_1 seam (dashed line in the figures) lies along the bond inversion one. According to the resulting topology, decay to the ground state can take place at the extended region of S_1/S_0 degeneracy, whereas recrossing to S_2 is possible because the seam of S_2/S_1 degeneracy must be passed before getting to the S_1/S_0 region.

The effect of dynamic correlation on the calculated results is shown in Figure 3c,d. Figure 3c presents the MEP, recalculated at CAS-PT2//CASSCF level of theory (see Computational Details). Because of the lowering of the energy of the (π,π^*) state, $(S_1)_{Min}$ has now (π,π^*) character. However, the mapping of the MEP at the CAS-PT2//CASSCF level shows that the MEP still goes through an S_2/S_1 crossing. When dynamic correlation is included, the position of $(S_2/S_1)_X$ is displaced further along the MEP and lies closer to $(S_1/S_0)_X$. In addition, the position of the triple crossing $(S_2/S_1/S_0)_X$ is displaced further along the bond inversion coordinate (see Figure 3d), and the associated S_1/S_0 and S_2/S_1 seams of intersection lie closer to each other than at the CASSCF level. Despite these changes in the topography, the main characteristics of the decay (extended region of S_1/S_0 degeneracy and possible recrossing to S_2 during the approach to the decay region), which are due to the interaction between the three relevant states, are the same when correlation energy is included.

Characterization of the Excited States and Vibronic Coupling. Analysis of the wave function is useful to characterize the relevant states and their role in the decay. In this context, our previous CASSCF study[11] indicated that the crossing responsible for the decay involved the ground state and the (n_O,π^*) state. In contrast to this, recent CAS-PT2 calculations[12] gave a different mechanistic picture because the CAS-PT2 energy of the (π,π^*) state is substantially lowered. As a consequence, the decay was described to involve the (π,π^*) and the ground state, essentially along the coordinate obtained at the CASSCF level, and a direct role of the (n_O,π^*) state was discarded. In the present study, the wave function was reanalyzed by including the three relevant states in the analysis. In this case, the states are found to be a mixture of the three relevant configurations (closed shell, (n_O,π^*), and (π,π^*)) at the region of decay (see Table 2 and Computational Details), due to the small energy gaps. The mixing of the (n_O,π^*) and (π,π^*) configurations along the pyramidalization coordinate reflects the proximity effect between the two excited states.

The vibronic coupling between the two states has been quantified, at the CASSCF level, at the geometry of the (π,π^*) state optimized at C_s symmetry (see Computational Details and Supporting Information). Our frequency analysis shows that the curvature of the (π,π^*) state along the pyramidalization mode is lowered by vibronic coupling with the (n_O,π^*) state. This effect is seen for the C_6 and N_1 pyramidalization coordinates, and the two atoms are pyramidalized at the decay point $(S_1/S_0)_X$ (by approximately 37 and 18°, respectively; see Table 1). This proves the importance of the proximity effect for the excited-state PES of cytosine.

Conclusions

The calculations discussed in the present paper strongly suggest that the potential energy surface in the region of radiationless decay of singly excited cytosine contains a 3-fold degeneracy between the ground state and the (π,π^*) and (n_O,π^*) excited states. Conceptually, the 3-fold degeneracy is the key feature of the surface because it is associated with seams of degeneracy between S_1 and S_0 and between S_2 and S_1, respectively. In first instance, the ultrafast decay of cytosine is due to the existence of an extended, energetically accessible S_1/S_0 seam along a combination of two geometric variables, a C_6 pyramidalization and a bond inversion coordinate. The lowest-energy part of the seam (centered around $(S_1/S_0)_X$, Figures 2 and 3) can be accessed after substantial C_6 pyramidalization (approximately 35°) and bond inversion (stretching of the C−O bond to approximately 1.42 Å). Decay at geometries with a higher bond inversion and less pyramidalization is also possible, although it requires more energy. Therefore, in a dynamic picture, decay is possible for different combinations of vibrational energy in the bond inversion and pyramidalization modes. In fact, dynamics calculations on the decay of fulvene,[28] the photochromism of a diaryl ethene model,[26] and the photoinduced cis−trans isomerization of a retinal chromophore model[27] confirm that decay to the ground state after photoexcitation can occur at different points along an S_1/S_0 seam of degeneracy, which in turn will influence the product distribution. However, in cytosine, the product yield is not affected by the place of decay because at the conical intersection $(S_1/S_0)_X$, the excited-state surface is flat[12] (intermediate topology of the intersection[37]), and regeneration of cytosine is the only ground-state decay path.

While the presence of the S_1/S_0 seam certainly accelerates the decay rate, the presence of an S_2/S_1 seam along the decay coordinate might slow it down because of recrossing to S_2 from the spectroscopically active S_1 state. In fact, the MEP shown in Figures 2 and 3 is a projection on one and two coordinates, and the MEP in the full space of coordinates will avoid the S_2/S_1 crossing. Nevertheless, the situation is similar to the one described for the photoisomerization of the chromophore of photoactive yellow protein, where a barrier on the S_1 surface lies very close to an S_2/S_1 crossing. Recrossing to S_2 (nonadia-

batic trapping) occurs in the ab initio excited-state dynamics of that molecule.[38] In analogy to these results, recrossing to S_2 also seems possible for cytosine.

From the point of view of which states are involved, decay from the Franck−Condon region leads to a mixed (π,π^*)/(n_O,π^*) state through vibronic coupling, rather than retaining the pure (π,π^*) character or switching to the (n_O,π^*) state. Thus, the excited-state species becomes progressively darker along the decay coordinate. This type of vibronic coupling (proximity effect) is usually termed pseudo-Jahn−Teller coupling, but this term is equivocal here because the coupling is associated with a conical intersection (i.e., a crossing of the S_1 and S_2 surfaces).

In the present work, we have focused on the topological features associated with the 3-fold degeneracy, mainly the doubly degenerate seams of intersection. However, little is known about the direct effect of a 3-fold crossing on the excited-state dynamics of general systems, not imposed by symmetry. Yarkony[21] has pointed out the possible effect of sequential, pairwise nonadiabatic transitions, which may reduce the overall efficiency of the decay. Moreover, in the present case, it is not clear if the triply degenerate space is accessible since the point located at the CAS-PT2 level is very high in energy. However, the corresponding CASSCF value is clearly below the vertical excitation energy. This may indicate that the CAS-PT2 value is overestimated and that the 3-fold degeneracy may be accessible in the real system. A further point that has to be considered is that the space of 3-fold degeneracy has a lower dimension (N-5) as compared to the 2-fold degenerate one (N-2). In any case, it is clear that dynamics calculations are needed to further clarify the picture. For the time being, our hypothesis is that the excited-state lifetime of cytosine (approximately 3.2 ps in the gas phase)[3] is the result of the balance between decay to the ground state and recrossing at the region of 3-fold degeneracy.

Acknowledgment. L.B. is financed by the Ramón y Cajal program from the Spanish Ministerio de Ciencia y Tecnología (MCyT) and by Grants BQU2002-04112-C02-02 and BQU2002-03334 from the Dirección General de Investigación (MCyT).

Supporting Information Available: Additional computational details and Cartesian geometries of the structures. This information is available free of charge via the Internet at http://pubs.acs.org.

References and Notes

(1) Callis, P. R. *Annu. Rev. Phys. Chem.* **1985**, *34*, 329−357.

(2) Crespo-Hernández, C. E.; Cohen, B.; Hare, P. M.; Kohler, B. *Chem. Rev.* **2004**, *104*, 1977−1202.

(3) Kang, H.; Lee, K. T.; Jung, B.; Ko, Y. J.; Kim, S. K. *J. Am. Chem. Soc.* **2002**, *124*, 12958−12959.

(4) Pecourt, J. M. L.; Peon, J.; Kohler, B. *J. Am. Chem. Soc.* **2000**, *122*, 9348−9349.

(5) Pecourt, J. M. L.; Peon, J.; Kohler, B. *J. Am. Chem. Soc.* **2001**, *123*, 10370−10378.

(6) Peon, J.; Zewail, A. H. *Chem. Phys. Lett.* **2001**, *348*, 255−262.

(7) Onidas, D.; Markovitsi, D.; Marguet, S.; Sharonov, A.; Gustavsson, T. *J. Phys. Chem. B* **2002**, *106*, 11367−11374.

(8) Nir, E.; Muller, M.; Grace, L. I.; de Vries, M. S. *Chem. Phys. Lett.* **2002**, *355*, 59−64.

(9) Malone, R. J.; Miller, A. M.; Kohler, B. *Photochem. Photobiol.* **2003**, *77*, 158−164.

(10) Sharonov, A.; Gustavsson, T.; Carre, V.; Renault, E.; Markovitsi, D. *Chem. Phys. Lett.* **2003**, *380*, 173−180.

(11) Ismail, N.; Blancafort, L.; Olivucci, M.; Kohler, B.; Robb, M. A. *J. Am. Chem. Soc.* **2002**, *124*, 6818−6819.

(12) Merchán, M.; Serrano-Andrés, L. *J. Am. Chem. Soc.* **2003**, *125*, 8108−8109.

(13) Shulepov, Y. V.; Pustovit, A. V. *Chem. Phys. Lett.* **1982**, *89*, 234−238.

(14) Keating, S. P.; Mead, C. A. *J. Chem. Phys.* **1985**, *82*, 5102−5117.

(15) Dixon, R. N. *Mol. Phys.* **1971**, *20*, 113−126.

(16) Katriel, J.; Davidson, E. R. *Chem. Phys. Lett.* **1980**, *76*, 259−262.

(17) Ceulemans, A.; Beyens, D.; Vanquickenborne, L. G. *J. Am. Chem. Soc.* **1984**, *106*, 5824−5837.

(18) Poliakoff, M.; Ceulemans, A. *J. Am. Chem. Soc.* **1984**, *106*, 50−54.

(19) Trushin, S. A.; Fuss, W.; Kompa, K. L.; Schmid, W. E. *J. Phys. Chem. A* **2000**, *104*, 1997−2006.

(20) Matsika, S.; Yarkony, D. R. *J. Am. Chem. Soc.* **2003**, *125*, 12428−12429.

(21) Matsika, S.; Yarkony, D. R. *J. Am. Chem. Soc.* **2003**, *125*, 10672−10676.

(22) Matsika, S.; Yarkony, D. R. *J. Chem. Phys.* **2002**, *117*, 7198−7206.

(23) Matsika, S.; Yarkony, D. R. *J. Chem. Phys.* **2002**, *117*, 6907−6910.

(24) Han, S. S.; Yarkony, D. R. *J. Chem. Phys.* **2003**, *119*, 11561−11569.

(25) Han, S. S.; Yarkony, D. R. *J. Chem. Phys.* **2003**, *119*, 5058−5068.

(26) Boggio-Pasqua, M.; Ravaglia, M.; Bearpark, M. J.; Garavelli, M.; Robb, M. A. *J. Phys. Chem. A* **2003**, *107*, 11139−11152.

(27) Weingart, O.; Migani, A.; Olivucci, M.; Robb, M. A.; Buss, V.; Hunt, P. *J. Phys. Chem. A* **2004**, *107*, 4685−4693.

(28) Bearpark, M. J.; Bernardi, F.; Olivucci, M.; Robb, M. A.; Smith, B. R. *J. Am. Chem. Soc.* **1996**, *118*, 5254−5260.

(29) Lai, T. I.; Lim, B. T.; Lim, E. C. *J. Am. Chem. Soc.* **1982**, *104*, 7631−7635.

(30) Broo, A. *J. Phys. Chem. A* **1998**, *102*, 526−531.

(31) Frisch, M. J.; Trucks, G. W.; Schlegel, H. B.; Scuseria, G. E.; Robb, M. A.; Cheeseman, J. R.; J. A. Montgomery, J.; Vreven, T.; Kudin, K. N.; Burant, J. C.; Millam, J. M.; Iyengar, S. S.; Tomasi, J.; Barone, V.; Mennucci, B.; Cossi, M.; Scalmani, G.; Rega, N.; Petersson, G. A.; Nakatsuji, H.; Hada, M.; Ehara, M.; Toyota, K.; Fukuda, R.; Hasegawa, J.; Ishida, M.; Nakajima, T.; Honda, Y.; Kitao, O.; Nakai, H.; Klene, M.; Li, X.; Knox, J. E.; Hratchian, H. P.; Cross, J. B.; Adamo, C.; Jaramillo, J.; Gomperts, R.; Stratmann, R. E.; Yazyev, O.; Austin, A. J.; Cammi, R.; Pomelli, C.; Ochterski, J. W.; Ayala, P. Y.; Morokuma, K.; Voth, G. A.; Salvador, P.; Dannenberg, J. J.; Zakrzewski, V. G.; Dapprich, S.; Daniels, A. D.; Strain, M. C.; Farkas, O.; Malick, D. K.; Rabuck, A. D.; Raghavachari, K.; Foresman, J. B.; Ortiz, J. V.; Cui, Q.; Baboul, A. G.; Clifford, S.; Cioslowski, J.; Stefanov, B. B.; Liu, G.; Liashenko, A.; Piskorz, P.; Komaromi, I.; Martin, R. L.; Fox, D. J.; Keith, T.; Al-Laham, M. A.; Peng, C. Y.; Nanayakkara, A.; Challacombe, M.; Gill, P. M. W.; Johnson, B.; Chen, W.; Wong, M. W.; Gonzalez, C.; Pople, J. A.; Gaussian 03 Revision B.02 ed.; Gaussian, Inc.: Pittsburgh, PA, 2003.

(32) Andersson, K.; Barysz, M.; Bernhardsson, A.; Blomberg, M. R. A.; Carissan, Y.; Cooper, D. L.; Cossi, M.; Fleig, T.; Fülscher, M. P.; Gagliardi, L.; Graaf, C. d.; Hess, B. A.; Karlström, G.; Lindh, R.; Malmqvist, P.-Å.; Neogrády, P.; Olsen, J.; Roos, B. O.; Schimmelpfennig, B.; Schütz, M.; Seijo, L.; Serrano-Andrés, L.; Siegbahn, P. E. M.; Stålring, J.; Thorsteinsson, T.; Veryazov, V.; Wierzbowska, M.; Widmark, P. O.; MOLCAS Version 5.4 ed.; University of Lund: Lund, Sweden, 2003.

(33) González, C.; Schlegel, H. B. *J. Phys. Chem.* **1990**, *94*, 5523−5527.

(34) Yarkony, D. R. *Faraday Discuss.* **2004**, *127*, 325−336.

(35) Bearpark, M. J.; Robb, M. A.; Schlegel, H. B. *Chem. Phys. Lett.* **1994**, *223*, 269−274.

(36) Bearpark, M. J.; Blancafort, L.; Robb, M. A. *Mol. Phys.* **2002**, *100*, 1735−1739.

(37) Atchity, G. J.; Xantheas, S. S.; Ruedenberg, K. *J. Chem. Phys.* **1991**, *95*, 1862−1876.

(38) Ko, C.; Levine, B.; Toniolo, A.; Manohar, L.; Olsen, S.; Werner, H. J.; Martinez, T. J. *J. Am. Chem. Soc.* **2003**, *125*, 12710−12711.